MODELLING STRONG ADVERSE PRESSURE GRADIENT FLOWS USING A TWO-LAYER REYNOLDS STRESS MODEL APPROACH

Yuri Laar
ONERA/Airbus Operations S.A.S.
F-31055 Toulouse, France
yuri.laar@onera.fr

François Chedevergne
DMPE, ONERA
F-31055 Toulouse, France
francois.chedevergne@onera.fr

Hervé Bézard
DMPE, ONERA
F-31055 Toulouse, France
herve.bezard@onera.fr

Aimad Er-Raiy
Airbus Operations S.A.S.
316 rte Bayonne Toulouse, France
aimad.er-raiy@airbus.com

ABSTRACT

Precise simulation of turbulent boundary layers in the presence of a strong adverse pressure gradient remains an essential challenge for industrial applications. Reynolds stress models (RSMs) provide an effective framework for addressing this; however, theoretical analysis of standard RSMs has highlighted certain shortcomings. Notable issues include the inaccurate prediction of the logarithmic layer slope and the failure to capture the square-root region when subjected to a strong adverse pressure gradient. To resolve these discrepancies, a two-layer elliptic blending model with a specific dissipation scale is proposed. The model successfully recovers key flow features, accurately predicting the slopes of both the logarithmic and square-root layers under strong adverse pressure gradient conditions.

INTRODUCTION

A primary challenge in aircraft design is to accurately and efficiently simulate complex industrial flows. To meet these demands, Airbus, ONERA and DLR introduced CODA (Stefanin Volpiani *et al.*, 2024), a new generation, computational fluid dynamics (CFD) solver. To succeed, models used in these simulations must preserve fundamental physics, particularly within the turbulent boundary layer (TBL). Because TBLs involve complex, multi-scale fluctuations, selecting and validating a robust turbulence model is essential.

Eddy Viscosity Models (Menter, 1994; Spalart & Allmaras, 1992) are commonly used for turbulence modelling in CFD. These models are computationally efficient but can exhibit weak prediction capabilities in complex flow situations. This study focuses on strong adverse pressure gradients (APG), which strongly influence both the mean flow profiles and the Reynolds stress distributions in turbulent boundary layers.

Inaccurate predictions in strong APG conditions highlight the limitations of standard models and motivate the search for advanced alternatives. This study relies on two state-of-the-art Reynolds-stress models: the SSG-LRR-ω model (Eisfeld *et al.*, 2016) and the Elliptic-Blending Model (EB-RSM) (Manceau, 2015). While the SSG-LRR-ω model utilizes a numerically robust specific dissipation-scale, ω, it struggles to accurately capture near-wall Reynolds profiles. Conversely, the EB-RSM relies on the dissipation-scale ε directly and lacks proper calibration for strong APG conditions. This study aims to develop an ω-based Reynolds stress model calibrated for strong APG conditions. The EB-RSM is selected as the baseline model due to its superior performance in estimating near-wall turbulence quantities.

TURBULENT BOUNDARY LAYERS UNDER STRONG ADVERSE PRESSURE GRADIENTS

A zero-pressure gradient turbulent boundary layer (TBL) is structured into an inner viscous region and an outer inertial region. At high Reynolds numbers, these are linked by a logarithmic layer where the velocity follows $\mathrm{U}^+ \propto \log \mathrm{y}^+$. In the viscous sublayer, the no-slip condition forces velocity to zero. The balance of viscous diffusion, dissipation, and pressure-strain redistribution (Pope, 2000) partially determines the damping of Reynolds stresses. Within the logarithmic zone, the mean velocity profile slope is defined from the von Kármán coefficient (κ), depending on an equilibrium between Reynolds stress production, dissipation, and pressure-strain redistribution (Durbin & Reif, 2010). This equilibrium starts to change when an adverse pressure gradient is introduced. The extent of the logarithmic zone decreases, and it becomes confined closer to the wall. The boundary layer under a strong adverse pressure gradient is illustrated in figure 1.

When the Clauser parameter $\beta = \frac{\delta^*}{\tau_w}\frac{\mathrm{d}P}{\mathrm{d}x} > 10$ (Townsend, 1980), a square-root zone emerges where velocity follows $\tilde{\mathrm{U}} \propto \sqrt{\tilde{\mathrm{y}}}$. Here, the velocity U and wall coordinate y are normalized by the pressure-based friction velocity u_p, indicated by the '$\tilde{}$' symbol. $\frac{\mathrm{d}P}{\mathrm{d}x}$ stands for the pressure gradient, τ_w the wall shear stress and δ^* the displacement thickness. Predicting this zone is essential for accurate CFD results.

$$\tilde{U} = \frac{2}{\kappa_{sq}}\sqrt{\tilde{y}}; \quad \tilde{y} = \frac{y u_p}{\nu}; \quad \tilde{U} = \frac{U}{u_p} \quad \text{with} \quad u_p = \left(\frac{\nu}{\rho}\frac{dp}{dx}\right)^{1/3} \tag{1}$$

Data from the Skåre and Krogstad diffuser (Krogstad & Skåre, 1995) yields a square-root slope of 0.28. This is close to the value of 0.31 of Knopp *et al.* (2021), though lower than the value of 0.45 found by Kader & Yaglom (1978) or 0.57

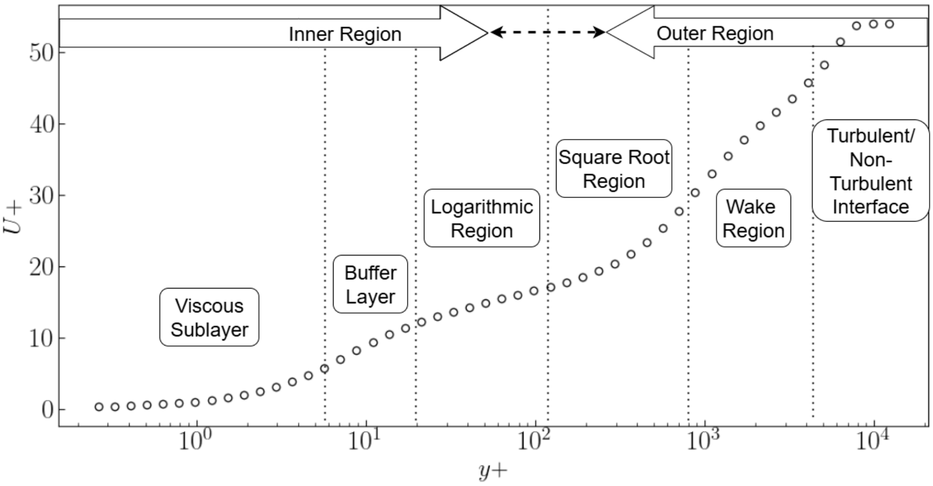

Figure 1: Regions in a boundary layer under a strong adverse pressure gradient

by Afzal (2008). In the outer region, wall constraints vanish and inertial effects dominate the wake zone and turbulent-non-turbulent interface. At the turbulent-non-turbulent interface, convection and turbulent diffusion reach equilibrium (Catris & Aupoix, 2000) as the flow reaches freestream conditions.

MODEL ANALYSIS

This study employs a theoretical framework based on boundary layer simplifications (Pope, 2000). By applying specific assumptions across different boundary layer zones, we establish and solve systems of equations to evaluate the performance of various turbulence models. These assumptions are summarized in Table 1.

In the viscous sublayer, the objective is to estimate the near-wall damping of the Reynolds stresses. This feature partly controls the correct peak of the Reynolds stresses in the buffer layer. Manceau & Hanjalić (2002) showed that their near-wall formulation of the pressure-strain term and the Rotta model (Rotta, 1951) for the dissipation tensor, with an ε-scale for the dissipation equation, provide a correct damping of the normal Reynolds stress tensor components. The current work considers an ω-scale, based on equation 4. The influence of this scale change is analyzed using power-law expansions of the turbulent variables based on the wall distance y. With these expansion coefficients α_q can be determined, as seen in table 1. Constant α_q determines how strongly the turbulent variables are damped near the wall, influenced by the equilibrium between viscous diffusion $D_{v_{ij}}$, the dissipation ε_{ij} and pressure-strain redistribution Π_{ij}. This analysis indicates that the Reynolds stresses are damped too strongly (eq. 2) with an ω-scale, as DNS data (Pope, 2000) indicates that $\overline{u'^2}, \overline{w'^2} \propto y^2$, $\overline{v'^2} \propto y^4$ and $\overline{u'v'} \propto y^3$.

$$\overline{u'^2}, \overline{w'^2} \propto y^{\frac{1+\sqrt{1+\frac{24\beta^*}{C_{\omega_2}}}}{2}} \propto y^{3.23}, \quad \overline{v'^2}, \overline{u'v'} \propto y^{\frac{1+\sqrt{1+\frac{144\beta^*}{C_{\omega_2}}}}{2}} \propto y^{7.10} \tag{2}$$

In the logarithmic region, the goal of the analysis is the estimation of the response to the pressure gradient of the Von Kármán constant (κ). To investigate the effects of a pressure-gradient on κ, Taylor series expansions on the turbulent variables are performed based on the pressure gradient. An analysis of near-wall conservation of momentum shows a correlation between p^+y^+, the wall-normalized pressure gradient and wall coordinate and $\overline{u'v'}^+$, the wall normalized Reynolds shear stress (Catris & Aupoix, 2000). The turbulent variables are expressed in the Taylor series expansion of the same variable (eq. 3). a_{ij} is the Reynolds anisotropy tensor and its Taylor series components. The main objective is to have a Von Kármán constant at zero pressure gradient (κ_0) of 0.39 and to have a Von Kármán constant that decreases with the pressure gradient ($\kappa_1 < 0$). These conditions are consistent with experimental data (Knopp *et al.*, 2021; Wu *et al.*, 2019; Lee & Sung, 2009).

$$-\overline{u'v'}^+ = 1 + p^+y^+ \quad a_{ij} = a_{ij_0} + a_{ij_1}p^+y^+, \quad \kappa = \kappa_0 + \kappa_1 p^+y^+ \tag{3}$$

A similar analysis, guided by different underlying physical principles, is performed for the square root layer. A different variable normalization based on p^+ allows an analysis with the goal of finding the right value of the slope of this region (κ_{sq}) (table 1). Coefficients A_q and r_q represent the Taylor series coefficient and power, respectively.

To properly model the outer region of a turbulent boundary layer, a model must both predict the wake and ensure the mean flow quantities transition smoothly at the boundary layer edge. This smoothness is essential to guarantee that the prediction is not overly sensitive to free-stream conditions. The analysis for the turbulent edge is conducted for a thin layer. For the longitudinal velocity profile, a self-similar form near the boundary edge is assumed. The mean flow and turbulence variables are expanded as powers of λ, a normalized wall coordinate. The values of the power coefficients control the smoothness of the solution reached at the edge of the TBL.

MODEL DESIGN AND CALIBRATION

While the EB-RSM accurately predicts Reynolds stress and mean flow profiles in zero-pressure gradient conditions (Manceau, 2015), its performance diminishes when subjected to strong adverse pressure gradients. The EB-RSM begins to underpredict the slope of the logarithmic layer and fails to predict the square-root zone (Sporschill *et al.*, 2022). Moreover, the ε-scale poses numerical robustness issues. The SSG-LRR-ω model struggles to accurately capture near-wall Reynolds stresses in a zero-pressure gradient flow. However, the ω-scale does provide numerical robustness. The aim is to mitigate the shortcomings of both models and design an ω-based elliptic

Region	RSM budget	Mean flow	Normalization	Turbulent var.	Visualization
Viscous sublayer	$D_{v_{ij}} + \Pi_{ij} - \varepsilon_{ij} = 0$	$U^+ = y^+$	$u_\tau = \sqrt{\frac{\tau_{wall}}{\rho}}$	$q = q_0 y^{\alpha_q}$	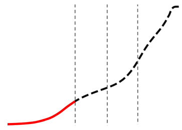
Logarithmic zone	$P_{ij} + \Pi_{ij} - \varepsilon_{ij} = 0$	$U^+ = \frac{1}{\kappa}\log(y^+) + B$	$u_\tau = \sqrt{\frac{\tau_{wall}}{\rho}}$	$q^+ = q_o + q_1 p^+ y^+$	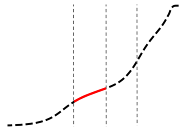
Square-root zone	$P_{ij} + \Pi_{ij} - \varepsilon_{ij} = 0$	$\tilde{U} = \frac{2}{\kappa_{sq}}\sqrt{\tilde{y}}$	$u_p = \left(\frac{\nu}{\rho}\frac{dp}{dx}\right)^{1/3}$	$\tilde{q} = A_q \tilde{y}^{r_q}$	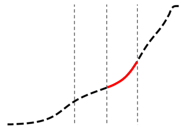
Boundary layer edge	$U_k \frac{\partial R_{ij}}{\partial x_k} = D^T_{ij}$	$U = U_{\text{ext}} - u_\tau F'(\lambda)$ $F' = F_{ext} - A_u \lambda^{e_u}$ $\lambda = 1 - \frac{y}{\delta}$	$u_\tau = \sqrt{\frac{\tau_{wall}}{\rho}}$	$Q = A_q \lambda^{e_q}$	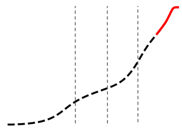

Table 1: Overview of the different assumptions in the analysis of different zones

blending model. This model is based on a generalized transport equation (eq. 4) for the specific dissipation. k represents the turbulence kinetic energy and P the production thereof. ν_t is the eddy viscosity, the C_{ij} are the model coefficients and $\beta^* = 0.09$. The present model introduces additional diffusion terms. These terms provide additional degrees of freedom to calibrate the model, notably regarding pressure gradient effects. The calibration of the model is based on the theoretical analysis presented in the previous section

A two-layer model was conceived, as a unique set of coefficients applicable across the whole boundary layer thickness cannot be achieved, even when considering all degrees of freedom. Actually, the outer region must be separated from the inner region to properly account for the growth of energy in the large-scale structures of a TBL in the presence of an APG (Harun *et al.*, 2013). The inner model correctly captures the behaviour of the viscous sublayer and the logarithmic zone, while the outer model accurately represents the square-root zone and the boundary layer edge. An optimization algorithm is used to find the right coefficients that fulfil all the requirements. The outcomes of the calibration are summarized in table 2.

$$\frac{D\omega}{Dt} = \frac{\omega}{k}(C_{\omega_1} P - C_{\omega_2}\varepsilon) + \frac{\partial}{\partial x_i}\left((C_V \nu + \frac{\nu_t}{C_\omega})\frac{\partial \omega}{\partial x_i}\right) + C_{\omega\omega}\frac{\nu_t}{\omega}\frac{\partial \omega}{\partial x_i}\frac{\partial \omega}{\partial x_i} + C_{\omega k}\frac{\nu_t}{k}\frac{\partial \omega}{\partial x_i}\frac{\partial k}{\partial x_i} + C_{kk}\frac{\nu_t \omega}{k^2}\frac{\partial k}{\partial x_i}\frac{\partial k}{\partial x_i} \tag{4}$$

A blending function is required to divide these two regions. Sporschill (2021) conceived a blending function based on the F1 function by Menter (1994). The function extends the viscous part of the blending function to the edge of the logarithmic zone. As this function appears to perform relatively well, it is also used in this model, albeit with a slight change of the constant, C_{zone}=2500. It reads:

$$f_{zone} = 1 - \tanh\left(\zeta^4\right), \quad \zeta = C_{zone}\frac{\nu}{\omega y^2} \tag{5}$$

To achieve the correct near-wall damping, C_V is introduced in the ω-equation (eq. 6). C_V serves as a damping coefficient on the viscous diffusion to compensate for the scale change. $C_V = 0.277$ leads to the correct damping of the normal Reynolds stresses (eq. 7). $\overline{u'v'}$ is still damped too strongly, but this is an inherent property of the Manceau and Hanjalić near-wall formulation of the pressure-strain term (Manceau, 2015). The boundary condition of ω also has to be corrected due to the changed viscous diffusion ($\omega_0 = C_V \frac{6\nu}{C_{\omega_2} y^2}$).

$$0 = -C_{\omega_2}\omega^2 + C_V \nu \frac{\partial^2 \omega}{\partial y^2} \tag{6}$$

$$\overline{u'^2}, \overline{w'^2} \propto y^{\frac{1+\sqrt{1+\frac{24 C_V \beta^*}{C_{\omega_2}}}}{2}} \propto y^2, \quad \overline{v'^2}, \overline{u'v'} \propto y^{\frac{1+\sqrt{1+\frac{144 C_V \beta^*}{C_{\omega_2}}}}{2}} \propto y^4 \tag{7}$$

In the logarithmic and square root regions, the dissipation equation coefficients are optimised to achieve the desired behaviour, following the model analysis procedure. No theoretical analysis is performed for the wake region, but careful optimisation of its production and dissipation coefficients is carried out. At the turbulent-non-turbulent interface, $e_u > 1$ is ensured. The model performance is summarised in Table 3.

Model	κ_0	κ_1	κ_{sq}	e_u^-	e_u^+
Two-Layer RSM	0.39	-0.06	0.28	2.0	2.34
Exp.	$\approx$ 0.39	$\approx$ -0.1	$\approx$ 0.28	1-15	1-15

Table 3: Perfomance of the newly conceived model

RESULTS

The model is validated for its intended use in high Reynolds number, turbulent flows with smooth geometry, such as those over wings and airfoils. The model should perform well both in zero-pressure gradient and strong pressure gradient flows. This study presents three test cases: a zero-pressure gradient flat plate and two windtunnel diffuser cases to investigate the impact of a strong adverse pressure gradient.

The simulations are performed with the new-generation Airbus-DLR-Onera CFD solver, CODA (Stefanin Volpiani *et al.*, 2024). The CODA simulations are performed using

	C_{ω_1}	C_{ω_2}	C_ω	C_{kk}	$C_{k\omega}$	$C_{\omega\omega}$
Inner layer model	0.440	0.0747	5.80	0.0	-0.74	0.69
Outer layer model	0.51	0.0696	2.21	0.71	-0.85	1.00

Table 2: Calibrated model constants

a second-order finite volume scheme with a Roe scheme for the convective part. To ensure numerical stability and avoid convergence issues, the transport equations for the turbulence variables are discretized using a first-order scheme.

Zero-Pressure Gradient Flow

Prior to addressing complex, pressure-gradient-driven flows, it is essential to validate the turbulence model's performance in the context of a turbulent boundary layer on a flat plate. The zero-pressure gradient flat plate case benchmarks the simulation of the Reynolds stress tensor components and ensures the proper development of a turbulent boundary layer. The model is compared to the EB-RSM, which gives satisfactory results for the flat plate case (Manceau, 2015). The case is set at $Re = 10^6$, based on a 2m plate and at a Mach number of 0.2. A comparative analysis of the friction coefficient for the flat plate case against Sillero's DNS data (Sillero *et al.*, 2013) is presented in Figure 2. The two-layer RSM demonstrates strong agreement with the reference data. These results suggest that the proposed model is well-suited for zero-pressure gradient conditions. Regarding the Reynolds stresses at $Re_\theta = 4040$ (Figure 3), the two-layer model slightly underpredicts the $\overline{v'v'}^+$ profile and slightly overpredicts the $\overline{u'u'}^+$ profile.

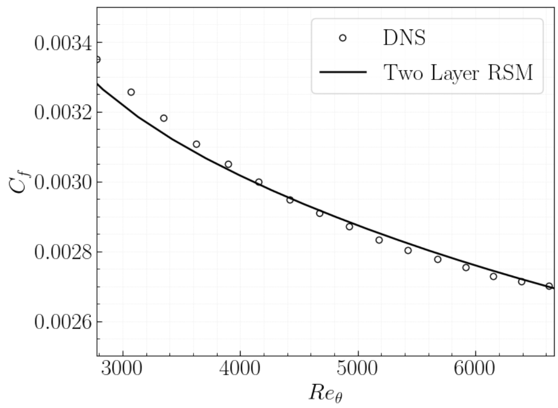

Figure 2: Comparison of skin friction progression on a flat plate compared to DNS data (Sillero *et al.*, 2013) (Mach = 0.2)

Skåre and Krogstad Diffuser

The Krogstad & Skåre (1995) setup is designed to investigate the response of a turbulent boundary layer to a sustained adverse pressure gradient. Through the use of a variable upper-wall profile, the experiment generates a strong adverse pressure gradient along the lower wall, pushing the flow near the separation point. Because it offers high-fidelity measurements of Reynolds stresses, mean velocities, and surface pressure, it remains a valuable benchmark for assessing the accuracy of turbulence models in adverse pressure gradient conditions.

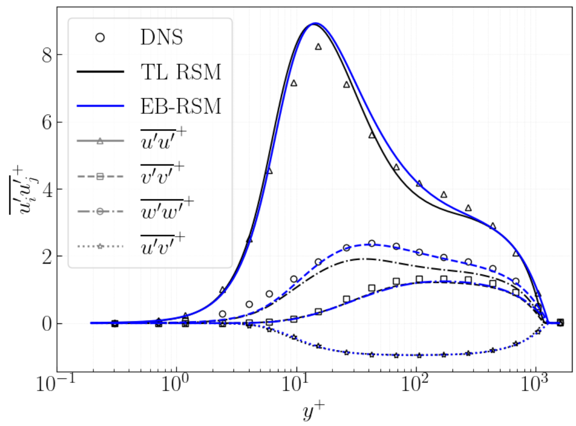

Figure 3: $\overline{u_i'u_j'}^+$ distribution (TL = Two Layer) on a flat plate compared to DNS data (Sillero *et al.*, 2013) (Re_θ = 4040, Mach = 0.2)

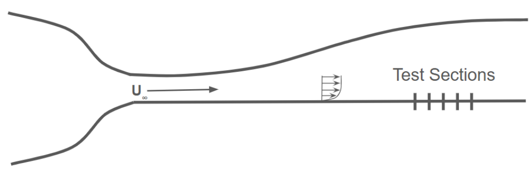

Figure 4: Illustration of the Skåre and Krogstad diffuser

Figure 5 shows the mean-flow results of the newly conceived model. The two-layer RSM model now predicts the logarithmic zone slope to steepen slightly at a von Kármán coefficient of 0.37, just as the model was designed to do. The square-root zone is also well represented with a von Kármán constant of 0.28. Figure 6 shows the Reynolds stress distributions at the last test section. The two-layer RSM model accurately depict the peak of kinetic energy in the buffer layer and the outer layer. The $\overline{v'v'}^+$ profile is slightly underestimated.

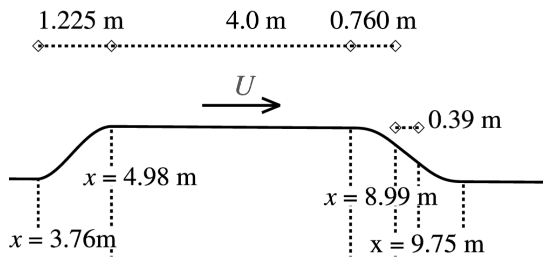

Figure 7: Illustration of the DLR/UniBw Experiment, recreated from (Knopp *et al.*, 2021)

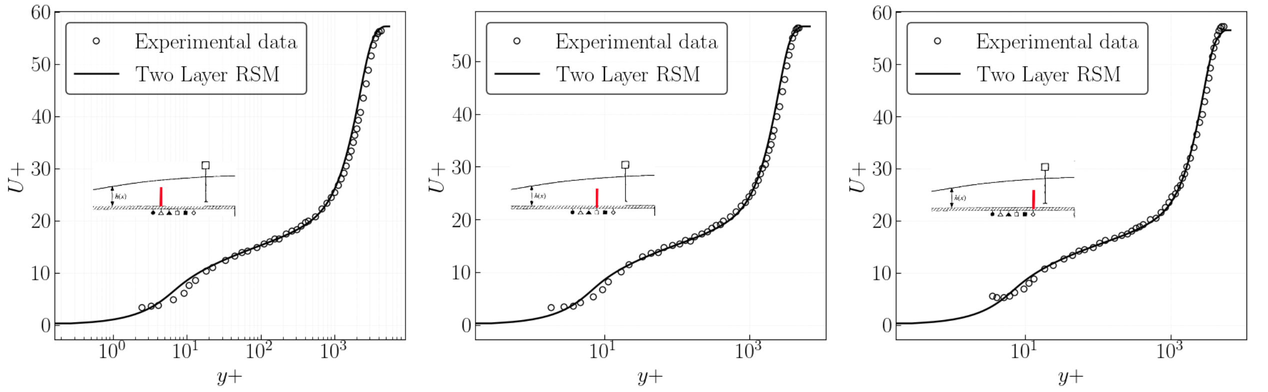

Figure 5: Mean flow Comparisons on the Skåre and Krogstad diffuser (Re_θ = [41580,46250,50980], β = [19.1,19.2,18.9])

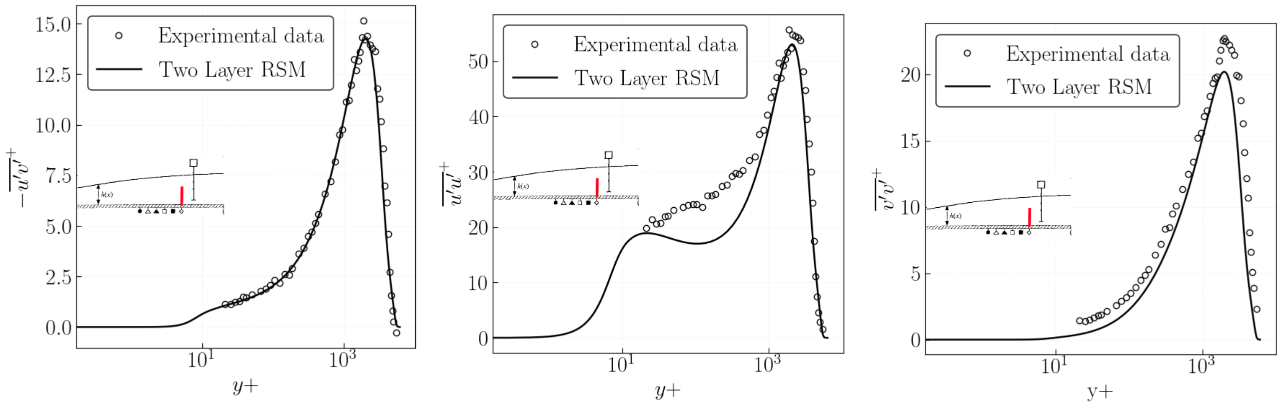

(a) Reynolds shear stress $\overline{u'v'}^+$ (b) Reynolds normal stress $\overline{u'u'}^+$ (c) Reynolds normal stress $\overline{v'v'}^+$

Figure 6: Reynolds stress distribution comparisons on the Skåre and Krogstad diffuser (Re_θ = 50980, β = 18.9)

DLR/UniBw Experiment

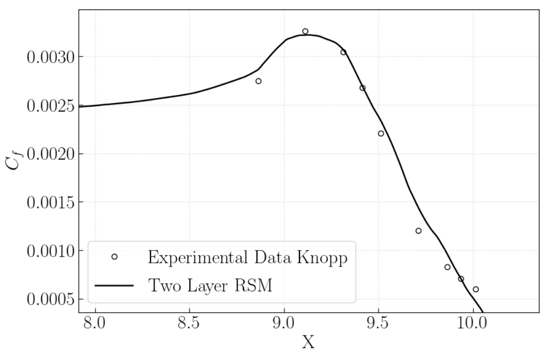

Figure 8: Skin friction coefficient progression on the DLR/UniBw experiment (Re = 25.1 million, Mach = 0.11)

An experimental investigation into adverse pressure gradient (APG) effects was conducted by Knopp *et al.* (2021) using a ramp-induced deceleration. This configuration drives the boundary layer towards separation, reaching $Re_\theta = 57363$ and a pressure gradient parameter $\beta = 26.37$ at the final measurement station. Unlike the equilibrium flows studied by Krogstad & Skåre (1995), the DLR/UniBw experiment involves a non-equilibrium boundary layer where spatial development significantly influences the flow physics. All measurements were taken at a subsonic Mach number of around 0.1.

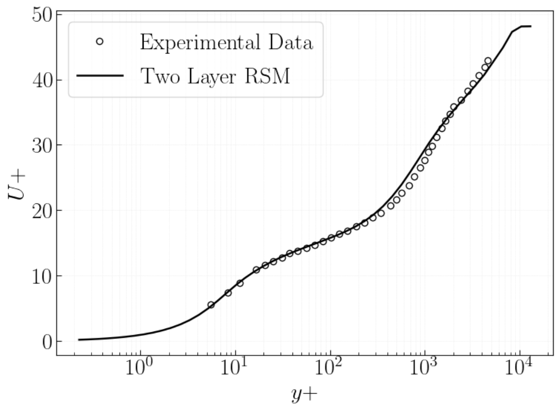

Figure 9: Mean flow Comparison on the DLR/UniBw experiment ($U_{inf} = 36$ m/s, Re_θ = 57363, β = 26.37)

Figure 8 tracks the skin friction coefficient across the test section. The two-layer RSM provides a reliable representation of the C_f progression under strong APG conditions; however, it deviates as separation approaches, resulting in an underestimation of the skin friction in that specific area. Figure 9 depicts the wall-normalized mean velocity profile at $X = 9.94$ m. The two-layer RSM again accurately predicts the different zones of the boundary layer. Both the slope of the logarithmic and square-root zones are well captured, despite a slight overestimation in the square root region. The model demonstrates strong overall performance in this APG case.

Conclusion

Accurately modelling turbulent boundary layers under strong adverse pressure gradients remains a critically important challenge for industrial applications. This can be effectively addressed by Reynolds stress models (RSMs). Particular limitations of the EB-RSM and SSG-LRR-ω models, are the incorrect prediction of the logarithmic layer slope and the absence of a square-root region when a strong adverse pressure gradient is encountered. To address these issues a two-layer elliptic blending model with a specific dissipation scale is proposed. This new model successfully predicts key flow features, including the correct slope of both the logarithmic and square-root layers under APG.

To enhance the model's robustness, future research will investigate its performance under compressibility, rotation, and favourable pressure gradients. Also, we can expect to reproduce similar effects obtained from the additional diffusion terms of equation 4 directly from a recalibration of the redistribution term, or by adding third order contributions to the SSG models. Such modifications, or a reinforcement of the present strategy may be deduced from a dissipation budget obtained from a DNS in an adverse pressure gradient configuration. However, so far, no such data were available.

REFERENCES

Afzal, Noor 2008 Turbulent Boundary Layer With Negligible Wall Stress. *Journal of Fluids Engineering* **130** (5), 051205.

Catris, Stéphane & Aupoix, Bertrand 2000 Towards a calibration of the length-scale equation. *International Journal of Heat and Fluid Flow* **21** (5), 606–613.

Durbin, P. A. & Reif, B. A. Pettersson 2010 *Statistical Theory and Modeling for Turbulent Flows*, 1st edn. Wiley.

Eisfeld, Bernhard, Rumsey, Chris & Togiti, Vamshi 2016 Verification and Validation of a Second-Moment-Closure Model. *AIAA Journal* **54** (5), 1524–1541.

Harun, Zambri, Monty, Jason P., Mathis, Romain & Marusic, Ivan 2013 Pressure gradient effects on the large-scale structure of turbulent boundary layers. *Journal of Fluid Mechanics* **715**, 477–498.

Kader, B. A. & Yaglom, A. M. 1978 Similarity treatment of moving-equilibrium turbulent boundary layers in adverse pressure gradients. *Journal of Fluid Mechanics* **89** (2).

Knopp, Tobias, Reuther, N., Novara, M., Schanz, D., Schülein, E., Schröder, A. & Kähler, C.J. 2021 Experimental analysis of the log law at adverse pressure gradient. *Journal of Fluid Mechanics* **918**, A17.

Krogstad, Per-Åge & Skåre, Per Egil 1995 Influence of a strong adverse pressure gradient on the turbulent structure in a boundary layer. *Physics of Fluids* **7** (8), 2014–2024.

Lee, Joung-Ho & Sung, Hyung Jin 2009 Structures in turbulent boundary layers subjected to adverse pressure gradients. *Journal of Fluid Mechanics* **639**, 101–131.

Manceau, Rémi 2015 Recent progress in the development of the Elliptic Blending Reynolds-stress model. *International Journal of Heat and Fluid Flow* **51**, 195–220.

Manceau, Rémi & Hanjalić, Kemal 2002 Elliptic blending model: A new near-wall Reynolds-stress turbulence closure. *Physics of Fluids* **14** (2), 744–754.

Menter, F. R. 1994 Two-equation eddy-viscosity turbulence models for engineering applications. *AIAA Journal* **32** (8), 1598–1605.

Pope, Stephen B. 2000 *Turbulent Flows*, 1st edn. Cambridge University Press.

Rotta, J. 1951 Statistische Theorie nichthomogener Turbulenz. *Zeitschrift fr Physik* **131** (1), 51–77.

Sillero, Juan A., Jiménez, Javier & Moser, Robert D. 2013 One-point statistics for turbulent wall-bounded flows at Reynolds numbers up to + 2000. *Physics of Fluids* **25** (10), 105102.

Spalart, P. & Allmaras, S. 1992 A one-equation turbulence model for aerodynamic flows. In *30th Aerospace Sciences Meeting and Exhibit*. Reno,NV,U.S.A.: American Institute of Aeronautics and Astronautics.

Sporschill, Gustave 2021 Improved Reynolds-Stress Modeling for Adverse-Pressure-Gradient Turbulent Boundary Layers in Industrial Aeronautical Flow. PhD thesis, Pau university, Pau.

Sporschill, Gustave, Billard, Flavien, Mallet, Michel, Manceau, Rémi & Bézard, Hervé 2022 Assessment of Reynolds-stress models for aeronautical applications. *International Journal of Heat and Fluid Flow* **96**, 108955.

Stefanin Volpiani, Pedro, Chapelier, Jean-Baptiste, Schwöppe, Axel, Jägersküpper, Jens & Champagneux, Steeve 2024 Aircraft Simulations Using the New CFD Software from ONERA, DLR, and Airbus. *Journal of Aircraft* **61** (3).

Townsend, Albert Alan 1980 *The structure of turbulent shear flow*, 2nd edn. Cambridge [GB] New York New Rochelle: Cambridge university press.

Wu, H., Moreau, S. & Sandberg, R. D. 2019 Effects of pressure gradient on the evolution of velocity-gradient tensor invariant dynamics on a controlled-diffusion aerofoil at. *Journal of Fluid Mechanics* **868**, 584–610.